Supporting Information for

The construction of dynamic dysprosium-carboxylate ribbons utilizing hybrid-ligands conception

Yu Fang,[a] Rong Sun,[b] Ai-Huan Sun,[a] Hao-Ling Sun*[a] and Song Gao*[b]

[a] *Department of Chemistry and Beijing Key Laboratory of Energy Conversion and Storage Materials, Beijing Normal University, Beijing 100875, P. R. China. E-mail: haolingsun@bnu.edu.cn;*

[b] *Beijing National Laboratory for Molecular Sciences, State Key Laboratory of Rare Earth Materials Chemistry and Applications, College of Chemistry and Molecular Engineering, Peking University, Beijing 100871, China. E-mail: gaosong@pku.edu.cn;*

Computational details

For complexes **1-3**, there is only one type of Dy^{3+} fragment, and thus we extracted one Dy^{3+} fragment (see Fig. 5 for the model structure of the calculated Dy^{3+} fragment) from **1-3** on the basis of single-crystal X-ray determined geometry. Complete-active-space self-consistent field (CASSCF) calculations on individual Dy^{3+} fragment have been carried out with MOLCAS 8.2 program package.[S1] The basis sets for all atoms are atomic natural orbitals from the MOLCAS ANO-RCC library: ANO-RCC-VTZP for Dy^{3+} ion; VTZ for close O and N; VDZ for distant atoms. During the calculation, the close Dy^{3+} ion was replaced by diamagnetic Lu^{3+}. The calculations employed the second order Douglas-Kroll-Hess Hamiltonian, where scalar relativistic contractions were taken into account in the basis set and the spin-orbit couplings were handled separately in the restricted active space state interaction (RASSI-SO) procedure. For the fragment of individual Dy^{3+} ion, active electrons in 7 active spaces include all *f* electrons (CAS (9 in 7)) in the CASSCF calculation. To exclude all the doubts, we calculated all the roots in the active space. We have mixed the maximum number of

spin-free state which was possible with our hardware (all from 21 sextets, 128 from 224 quadruplets, 130 from 490 doublets).

Fitting the exchange interaction in two complexes using Lines model based on CASSCF results

To fit the exchange interactions in complex **1-3**, we took two steps to obtain them. Firstly, we calculated the mononuclear fragment using CASSCF to obtain the corresponding magnetic properties (see the first part). And then, the exchange interaction between the magnetic centers is considered within the Lines model,[S2] while the account of the dipole-dipole magnetic coupling is treated exactly. The Lines model is effective and has been successfully used widely in the research field of binuclear lanthanide single-molecule magnets.[S3]

For complex **1-3**, we only consider one type of Dy^{3+}- Dy^{3+} interactions. The exchange Hamiltonian can be expressed as follow: $\widehat{H}_{exch} = -J^{total}\hat{S}_{Dy1}\hat{S}_{Dy2}$

The J_{total} is the parameter of the total magnetic interaction (J_{total}=$J_{dipolar}$+$J_{exchange}$) between Dy^{3+} ions. The $\hat{S}_{Dy}$ = ±1/2 is the ground pseudospin on the Dy^{3+} site. The dipolar magnetic coupling can be calculated exactly, while the exchange coupling constant was fitted through comparison of the computed and measured magnetic susceptibility using the POLY_ANISO program.[S4]

Table S1. Selected Bond Distances (Å) in complex **1-3**.

	1	**2**	**3**
Dy-N1	2.489	2.486	2.490
Dy-N2	2.568	2.610	2.561
Dy-O1	2.333	2.340	2.320
Dy-O2	2.356	2.362	2.368
Dy-O3	2.337	2.342	2.367
Dy-O3#2	2.621	2.585	2.547
Dy-O4	2.433	2.475	2.452
Dy-O5	2.564	2.498	2.388
Dy-O6	2.388	2.398	2.423

Table S2. Hydrogen Bonds in **1**.

D-H	d(D-H) (Å)	<DHA (°)	d(D…A) (Å)	A
C10-H10	1.065	159.92	2.601	O5 [-1-x, -1-y, -z]
C7-H7	0.930	154.29	2.403	O6 [-3-x, -1-y, -z]

Table S3. Hydrogen Bonds in **2**.

D-H	d(D-H) (Å)	<DHA (°)	d(D…A) (Å)	A
O2-H2A	0.850	163.58	2.601	O5 [2-x, 1-y, 1-z]
O2-H2B	0.850	167.74	2.681	O1 [1+x, y, -z]
C4-H4	0.930	125.58	3.133	O4[2-x, 0.5+y,1.5-z]
C7-H7	0.930	151.12	3.314	O6[2-x, 0.5+y,1.5-z]

Table S4. Hydrogen Bonds in **3**.

D-H	d(D-H) (Å)	<DHA (°)	d(D…A) (Å)	A
O2-H2a	0.875	144.35	2.699	O5 [-1+x, y, z]
C8-H8	0.930	155.23	3.396	O4 [4-x, 1-y, 1-z]

Table S5. Relaxation fitting parameters from Least-Squares Fitting of $\chi(f)$ data under zero dc field and 3 kOe dc field of **1**.

1 under zero dc field				
T (K)	χ_T	χ_S	α	τ (s)
2	5.000	0.855	0.312	0.0358
2.5	4.321	0.694	0.321	0.0355
3	3.718	0.633	0.297	0.0353
3.5	3.269	0.557	0.295	0.0347
4	2.925	0.502	0.293	0.0342
4.5	2.640	0.454	0.291	0.0339
5	2.417	0.414	0.292	0.0329
5.5	2.211	0.389	0.279	0.0319
6	2.004	0.393	0.236	0.0299
6.5	1.850	0.372	0.212	0.0266
7	1.714	0.352	0.185	0.0182
7.5	1.585	0.344	0.142	0.0139
8	1.473	0.350	0.090	0.0103
8.5	1.389	0.333	0.073	0.0072
9	1.311	0.325	0.046	0.0049
9.5	1.242	0.328	0.018	0.0033
10	1.188	0.276	0.039	0.0020
10.5	1.136	0.258	0.044	0.0012
11	1.085	0.258	0.023	7.25E-4
11.5	1.002	0.077	0.148	3.63E-4
12	1.042	0.070	0.172	2.24E-4
12.5	0.987	0.070	0.149	1.27E-4
13	0.855	0.089	0.067	7.55E-5
13.5	0.819	0.096	0.047	4.76E-5
14	0.793	0.087	0.058	3.00E-5
14.5	0.768	0.072	0.070	1.88E-5
15	0.741	0.091	0.059	1.30E-5
15.5	0.718	0.112	0.058	9.11E-6
16	0.696	0.142	0.057	6.65E-6
1 under 3 kOe dc field				
T (K)	χ_T	χ_S	α	τ (s)
6	2.183	0.325	0.280	0.1930
6.5	1.867	0.322	0.200	0.1019
7	1.696	0.268	0.236	0.0667
7.5	1.586	0.266	0.166	0.0358
8	1.471	0.250	0.143	0.0214
8.5	1.362	0.255	0.088	0.0130
9	1.290	0.237	0.083	0.0079

9.5	1.220	0.246	0.040	0.0048
10	2.091	0.050	0.307	0.0097
10.5	1.336	0.056	0.236	0.0024
11	1.091	0.061	0.178	9.81E-4
11.5	0.974	0.066	0.134	4.91E-4
12	0.916	0.069	0.109	2.70E-4
12.5	0.868	0.073	0.086	1.55E-4
13	0.836	0.073	0.081	9.13E-5
13.5	0.808	0.070	0.084	5.47E-5
14	0.785	0.051	0.106	3.26E-5
14.5	0.759	0.036	0.113	1.96E-5
15	0.759	0.028	0.113	1.23E-5
15.5	0.713	0.007	0.123	7.59E-6
16	0.691	0.021	0.123	5.16E-6

Table S6. Relaxation fitting parameters from Least-Squares Fitting of $\chi(f)$ data under zero dc field and 3 kOe dc field of **2**.

2 under zero dc field				
T (K)	χ_T	χ_S	α	τ (s)
2	4.571	0.500	0.398	0.0071
2.5	3.906	0.418	0.395	0.0076
3	3.407	0.360	0.397	0.0079
3.5	3.015	0.320	0.398	0.0079
4	2.696	0.294	0.398	0.0078
4.5	2.435	0.276	0.396	0.0075
5	2.218	0.262	0.392	0.0070
5.5	2.029	0.255	0.382	0.0064
6	1.865	0.251	0.368	0.0057
6.5	1.726	0.252	0.345	0.0050
7	1.598	0.254	0.314	0.0042
7.5	1.484	0.260	0.272	0.0034
8	1.391	0.262	0.234	0.0027
8.5	1.305	0.267	0.186	0.0020
9	1.234	0.269	0.145	0.0015
9.5	1.169	0.275	0.099	0.0010
10	1.115	0.271	0.077	6.67E-4
10.5	1.062	0.282	0.042	4.39E-4
11	1.048	0.127	0.206	2.07E-4
11.5	0.987	0.125	0.171	1.21E-4
12	0.926	0.145	0.098	7.65E-5
12.5	0.877	0.154	0.060	4.98E-5
13	0.844	0.154	0.051	3.25E-5
13.5	0.811	0.180	0.018	2.30E-5
14	0.788	0.137	0.053	1.41E-5
2 under 3 kOe dc field				
T (K)	χ_T	χ_S	α	τ (s)
6	1.920	0.142	0.262	0.1374
6.5	1.798	0.134	0.245	0.0849
7	1.605	0.131	0.199	0.0490
7.5	1.439	0.144	0.127	0.0273
8	1.352	0.132	0.124	0.0162
8.5	1.269	0.139	0.098	0.0095
9	1.199	0.141	0.083	0.0055
9.5	1.149	0.110	0.121	0.0030
10	1.090	0.118	0.102	0.0016
10.5	1.042	0.126	0.095	9.12E-4
11	1.037	0.095	0.196	4.48E-4

11.5	0.964	0.094	0.178	2.32E-4
12	0.891	0.104	0.130	1.22E-4
12.5	0.874	0.093	0.151	7.04E-5
13	0.839	0.105	0.124	4.21E-5
13.5	0.789	0.148	0.053	2.88E-5
14	0.775	0.117	0.095	1.70E-5
14.5	0.757	0.017	0.146	8.60E-6

Table S7. Relaxation fitting parameters from Least-Squares Fitting of $\chi(f)$ data under zero dc field and 3 kOe dc field of **3**.

3 under zero dc field				
T (K)	χ_T	χ_S	α	τ (s)
2	5.935	0.945	0.209	0.0050
2.5	4.922	0.788	0.196	0.0049
3	4.215	0.677	0.195	0.0049
3.5	3.675	0.600	0.192	0.0047
4	3.251	0.544	0.186	0.0045
4.5	2.906	0.531	0.164	0.0042
5	2.644	0.487	0.164	0.0040
5.5	2.418	0.415	0.170	0.0028
6	2.193	0.540	0.079	0.0025
6.5	2.027	0.546	0.052	0.0019
7	1.90	0.388	0.117	0.0012
7.5	1.771	0.409	0.082	9.00E-4
8	1.669	0.411	0.078	6.47E-4
8.5	1.573	0.426	0.062	4.58E-4
9	1.483	0.460	0.037	3.22E-4
9.5	1.409	0.483	0.034	2.14E-4
10	1.381	0.196	0.188	9.92E-5
10.5	1.291	0.212	0.148	5.58E-5
11	1.234	0.216	0.134	3.69E-5
11.5	1.169	0.245	0.103	2.28E-5
12	1.122	0.294	0.074	1.65E-5
12.5	1.075	0.290	0.081	9.91E-6
13	1.038	0.327	0.067	7.39E-6
3 under 3 kOe dc field				
4	3.441	0.117	0.400	0.1070
4.5	2.915	0.118	0.347	0.0509
5	2.546	0.124	0.291	0.0259
5.5	2.285	0.130	0.247	0.0144
6	2.088	0.142	0.204	0.0086
6.5	1.933	0.158	0.168	0.0054
7	1.804	0.172	0.141	0.0035
7.5	1.700	0.183	0.127	0.0023
8	1.6	0.199	0.109	0.0015
8.5	1.516	0.213	0.106	9.45E-4
9	1.446	0.230	0.117	5.95E-4
9.5	1.377	0.264	0.126	3.67E-4
10	1.354	0.104	0.251	1.94E-4
10.5	1.271	0.097	0.252	9.54E-5

11	1.205	0.096	0.247	5.40E-5
11.5	1.150	0.087	0.247	2.70E-5
12	1.103	0.101	0.238	1.65E-5
12.5	1.057	0.140	0.221	9.72E-6
13	1.025	0.098	0.245	5.50E-6

Table S8. Calculated energy levels (cm^{-1}) and ***g*** (g_x, g_y, g_z) tensors of the lowest Kramers doublets (KDs) of individual Dy^{3+} fragment of complexes **1-3**.

KDs	**1**		**2**		**3**	
	E/cm^{-1}	***g***	*E*/cm^{-1}	***g***	*E*/cm^{-1}	***g***
1	0.0	0.01 0.04 19.41	0.0	0.04 0.09 19.58	0.0	0.07 0.16 19.59
2	88.8	0.51 0.76 17.30	85.2	0.25 0.38 18.68	53.2	0.09 0.30 19.37
3	142.8	2.06 3.43 12.50	152.0	2.17 3.68 13.58	162.5	3.12 5.54 12.43
4	200.0	8.83 6.76 3.27	197.1	10.19 6.16 1.66	190.6	0.15 4.99 10.92
5	242.9	0.23 2.11 13.91	243.8	1.20 3.73 12.79	225.7	2.51 3.72 12.81
6	278.6	8.24 6.95 1.93	284.7	0.60 1.25 15.04	312.7	0.64 1.12 14.33
7	293.8	10.45 6.98 2.19	317.7	0.17 0.56 16.47	374.2	0.20 0.29 18.45
8	371.3	0.14 0.27 18.94	397.2	0.01 0.07 19.15	426.6	0.06 0.20 18.80

Table S9. Wave functions with definite projection of the total moment | m_J > for the lowest three Kramers doublets (KDs) of individual Dy^{3+} fragments for complexes **1-3**. The principal axes frame is aligned with that of the ground state g tensor.

	E/cm^{-1}	wave functions
1	0.0	94%|±15/2>
	88.8	+19%|±5/2>+21%|±3/2>+20%|±1/2>
	142.8	50%|±13/2>++11%|±9/2>+12%|±7/2>+
2	0.0	96%|±15/2>
	85.2	21%|±7/2>+22%|±5/2>+19%|±3/2>
	152.	57%|±13/2>+14%|±11/2>+12%|±7/2>

	0	
3	0.0	97%|±15/2>
	53.2	23%|±9/2>+22%|±7/2>+18%|±5/2>
	162.5	54%|±13/2>+11%|±9/2>+14%|±7/2>

Table S10. Fitted exchange coupling constant J_{exch}, the calculated dipole-dipole interaction $J_{dipolar}$ and the total J_{total} between two Dy^{3+} ions with the shorter distance in complexes **1-3** (cm^{-1}). The intermolecular interaction zJ' of **1-3** was fit to 0.00 cm^{-1}.

	1	**2**	**3**
$J_{dipolar}$	−0.80	-0.91	-1.17
J_{exch}	-2.25	-0.75	-0.50
J_{total}	-3.05	-1.66	-1.67

Table S11. The included angles θ between the magnetic axes of Dy^{3+} ion and the vector connecting two Dy^{3+} ions within the dimer of complexes **1-3**.

Complex	**1**	**2**	**3**
θ / º	117.8	116.8	114.4

Table S12. Reported nine-coordinated carboxylate Dy^{3+} molecule nanomagnets.

Complexes	Structure	U_{eff} / K	Dc field / Oe	Ref.
$[Dy(2\text{-py-}4\text{-pmc})(L_1)(H_2O)]$	1D	180	0	this work
$[Dy(2\text{-py-}4\text{-pmc})(L_2)(H_2O)]$	1D	145		
$[Dy(2\text{-py-}4\text{-pmc})(L_3)(H_2O)]$	1D	137		
$[Dy_2(INO)_4(NO_3)_2]\cdot 2CH_3CN$	3D	110	0	8a
$[Dy_2(NO_3)_4(sacbH)_2(H_2O)_2(MeCN)_2]$	binuclear	109	0	8b
$[Dy_2(\mu2\text{-anthc})_4(anthc)_2(L_1)_2]$	binuclear	52	0	8c
$[Dy_2(\mu2\text{-anthc})_4(anthc)_2(L_2)_2]$	binuclear	32		
$[Dy_2(\mu2\text{-anthc})_4(anthc)_2(L_3)_2]$	binuclear	49		
$[Dy_2(H_3L)_2(PhCOO)_4]\cdot 4H_2O$	binuclear	43	0	8d
$[Dy_2(L_2)_2(OX)_2(H_2O)]\cdot 2H_2O$	3D	38	2000	8e
$[Dy(L_2)_3(DMSO)]_n$	1D	14	900	8f
$[Dy_2(1\text{-tza})_4(NO_3)_2(2,2'\text{-bipy})_2]$	binuclear	42	2000	8g
$[Dy(C_2O_4)_{1.5}(H_2O)_3]_n\cdot 2nH_2O$	2D	11	700	8h

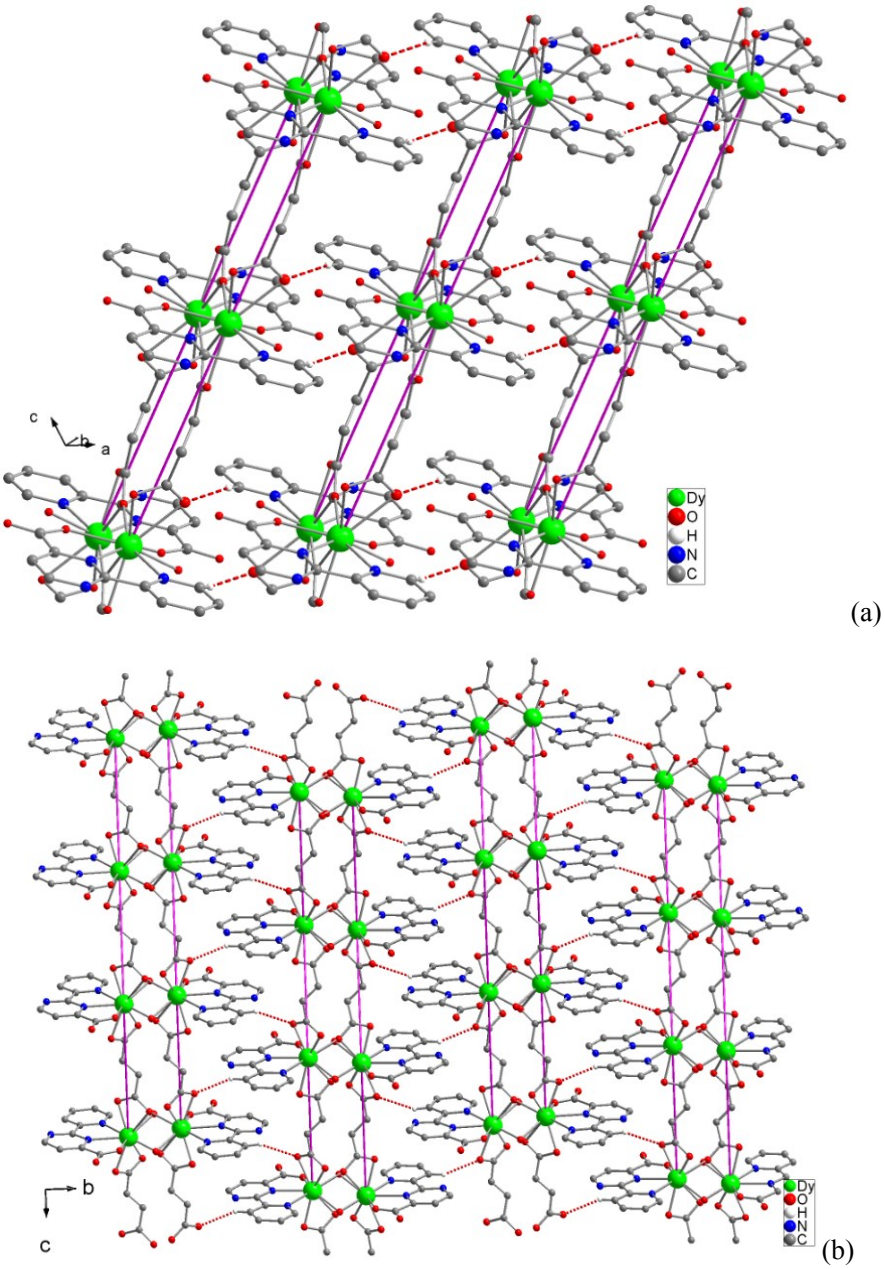

Fig. S1 The hydrogen-bonded 2D layer (a) and the connection of the hydrogen bonds between the layers (b) in **1**.

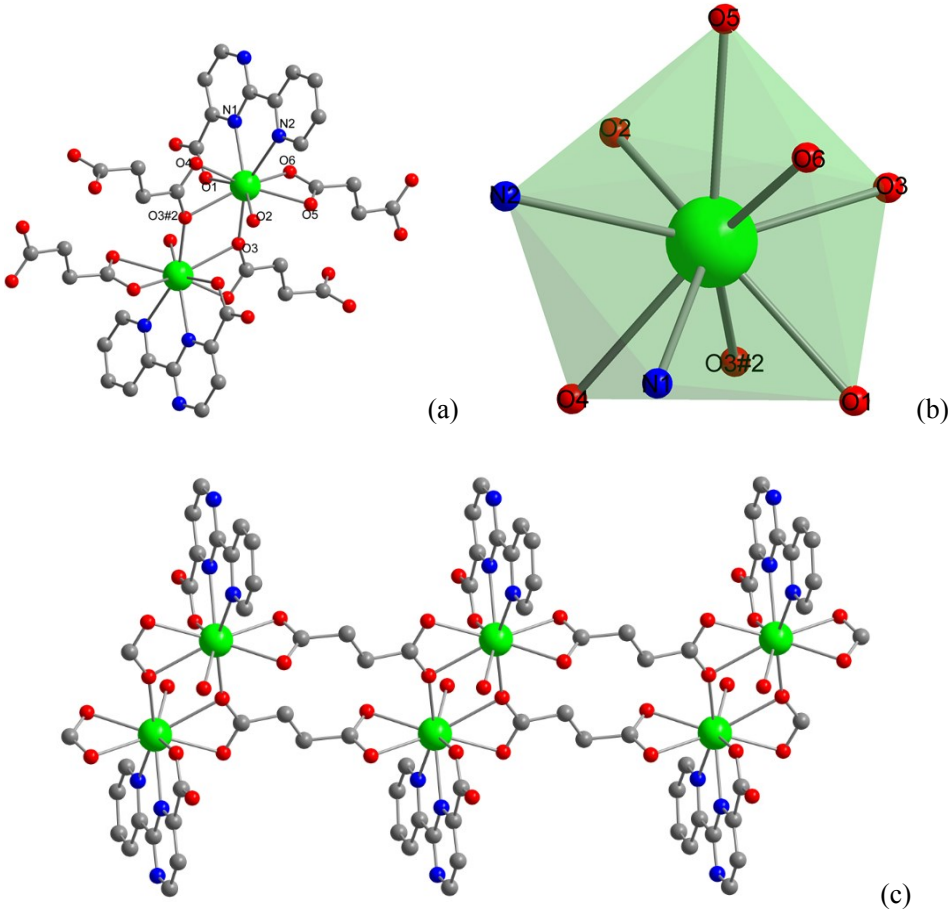

Fig. S2 The local structure (a), coordination polyhedron around Dy^{3+} ion (b) and double-chain structure (c) of complex **2**. Hydrogen atoms and solvent molecules are omitted for clarity.

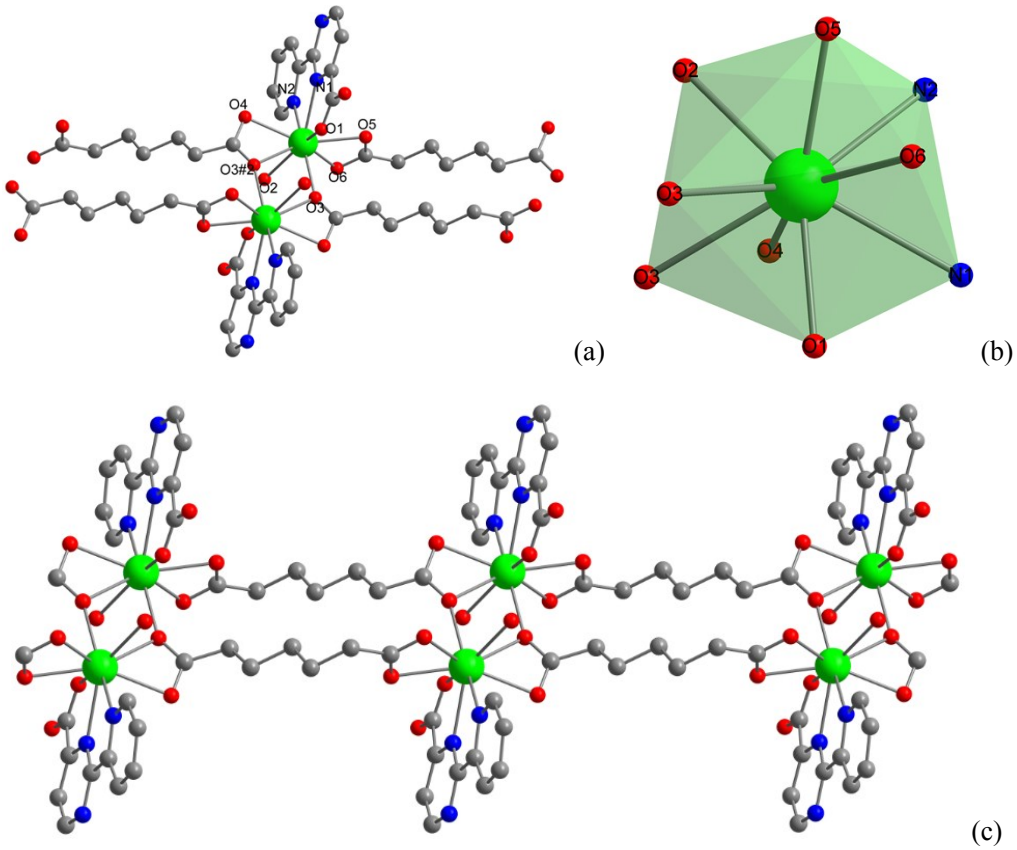

Fig. S3 The local structure (a), coordination polyhedron around Dy^{3+} ion (b) and double-chain structure (c) of complex **3**. Hydrogen atoms and solvent molecules are omitted for clarity.

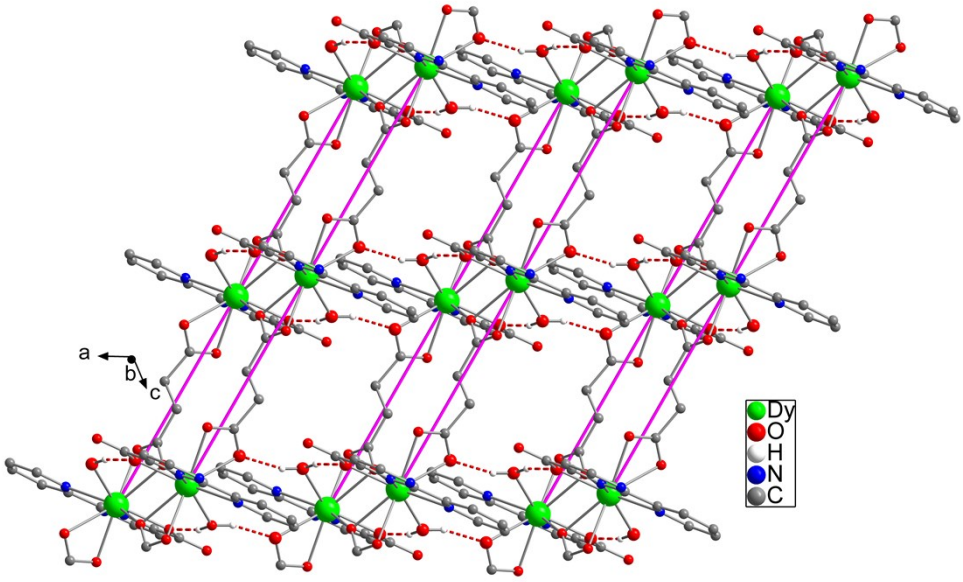

(a)

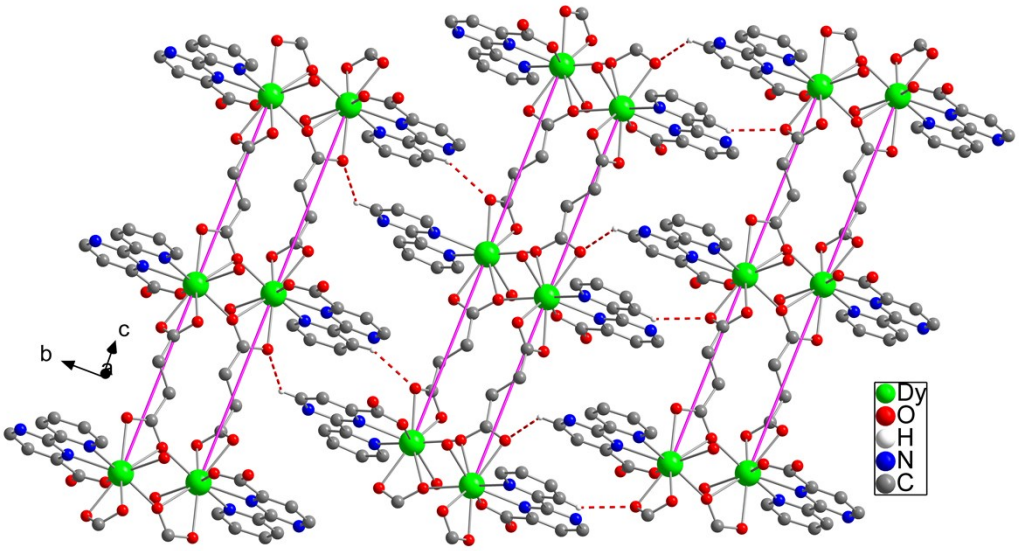

(b)

Fig. S4 The hydrogen-bonded 2D layer (a) and the connection of the hydrogen bonds between the layers (b) in **2**.

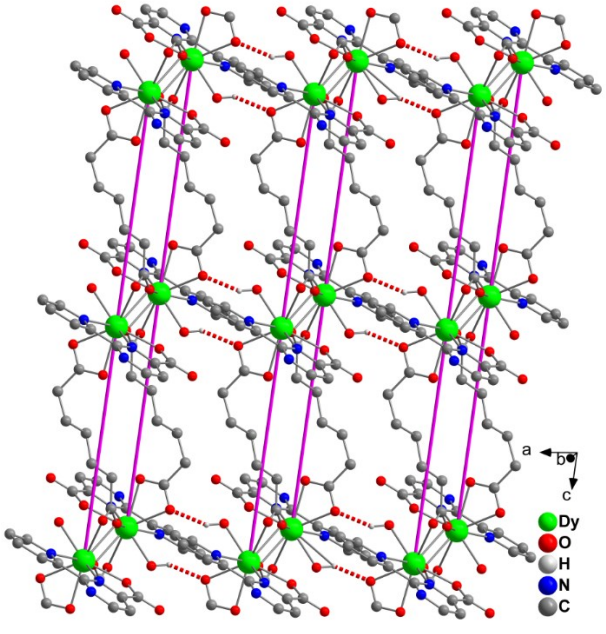

(a)

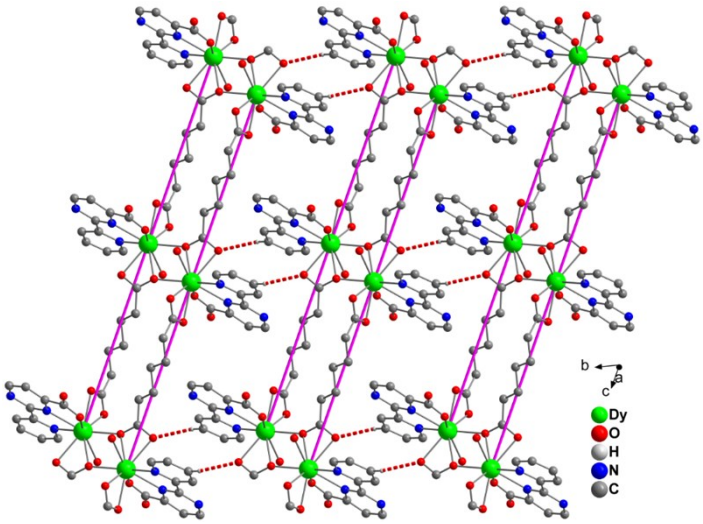

(b)

Fig. S5 The hydrogen-bonded 2D layer (a) and the connection of the hydrogen bonds between the layers (b) in **3**.

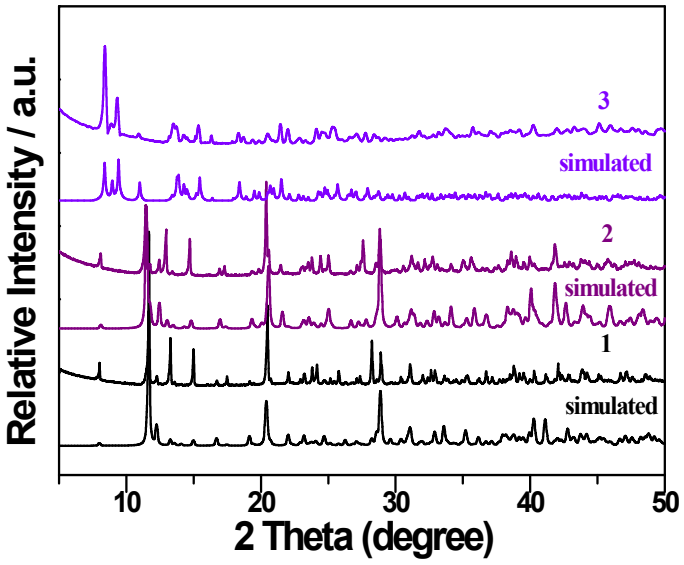

Fig. S6 Powder X-ray diffraction profiles of **1-3** together with a simulation from the single crystal data.

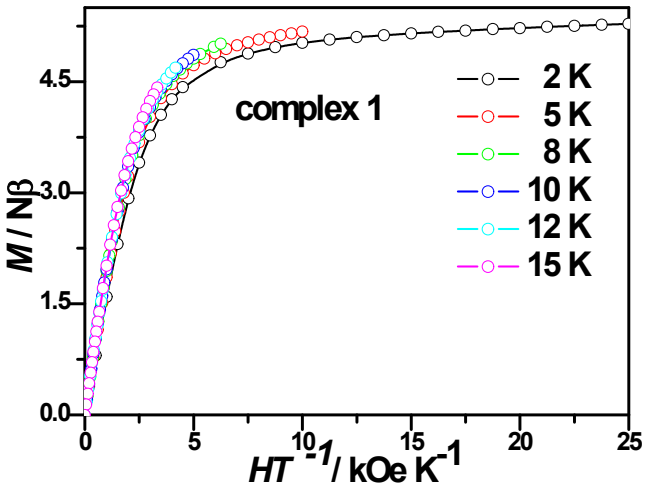

(a)

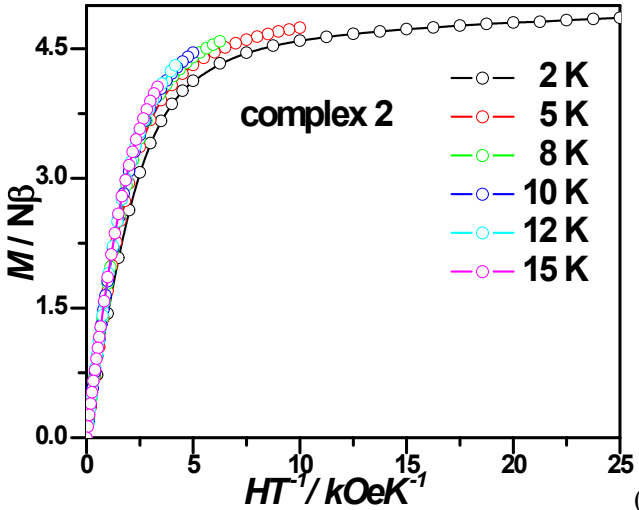

(b)

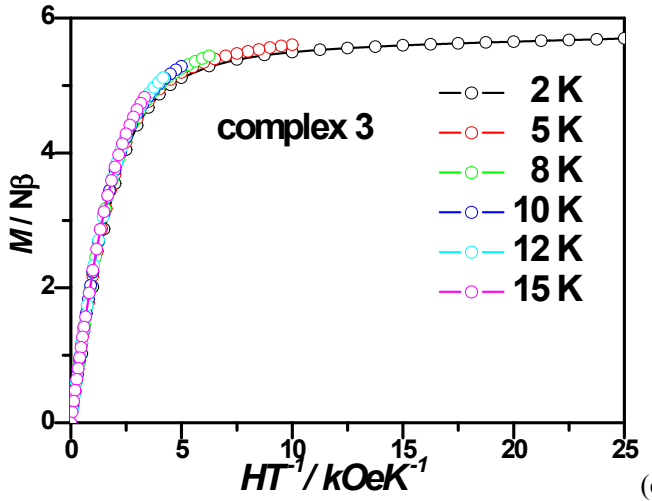

(c)

Fig. S7 Plots of *M-H/T* at 2, 5, 8, 10, 12 and 15 K for **1-3**.

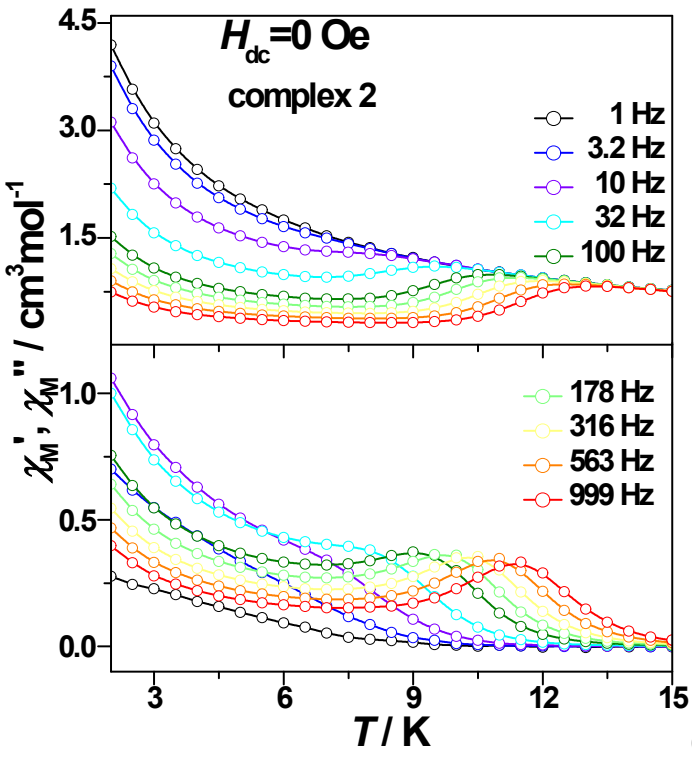

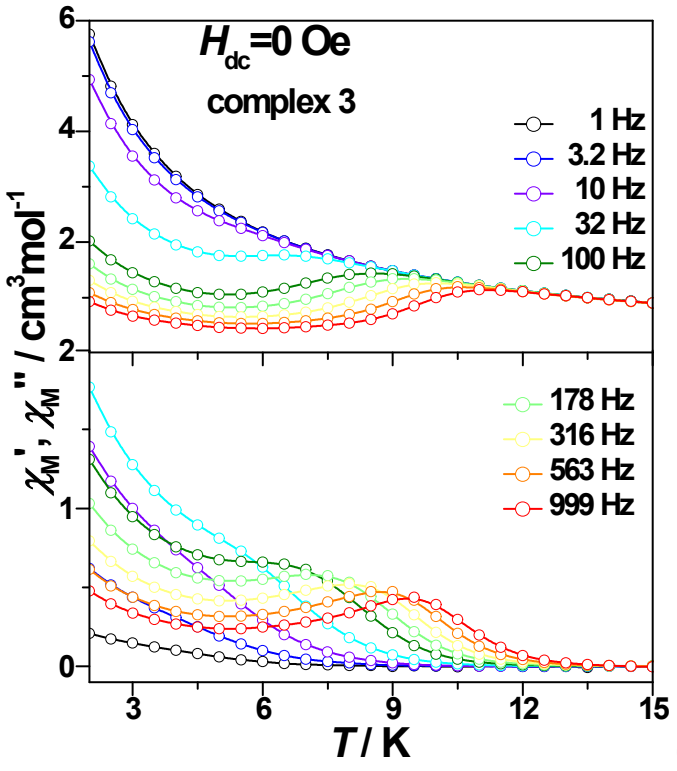

Fig. S8 Temperature dependence of the in-phase χ_M' (top) and out-of-phase χ_M'' (bottom) ac signals under zero dc field for complex **2** (a) and **3** (b).

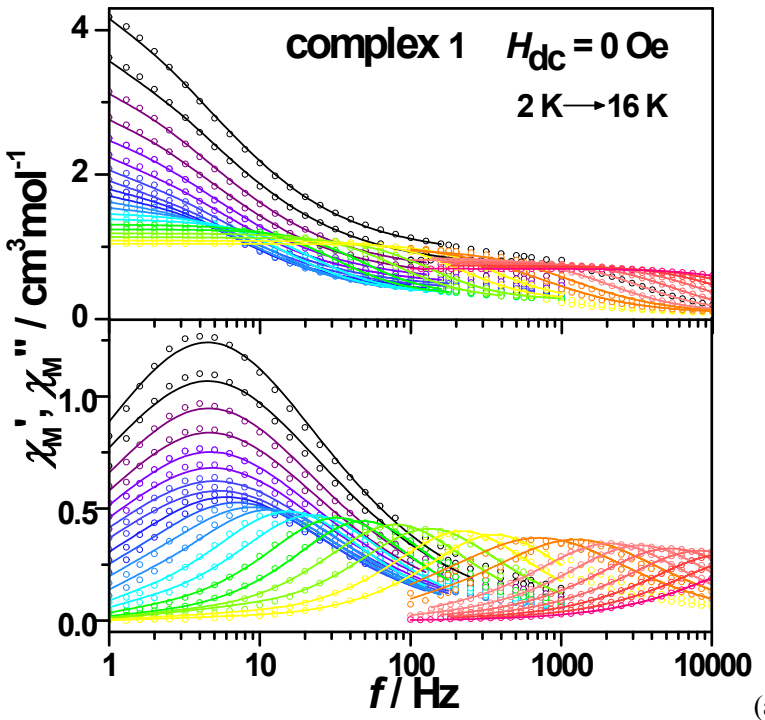
complex 1
H_{dc} = 0 Oe
2 K→16 K
χ_M', χ_M'' / cm^{3}mol^{-1}
f / Hz

(a)

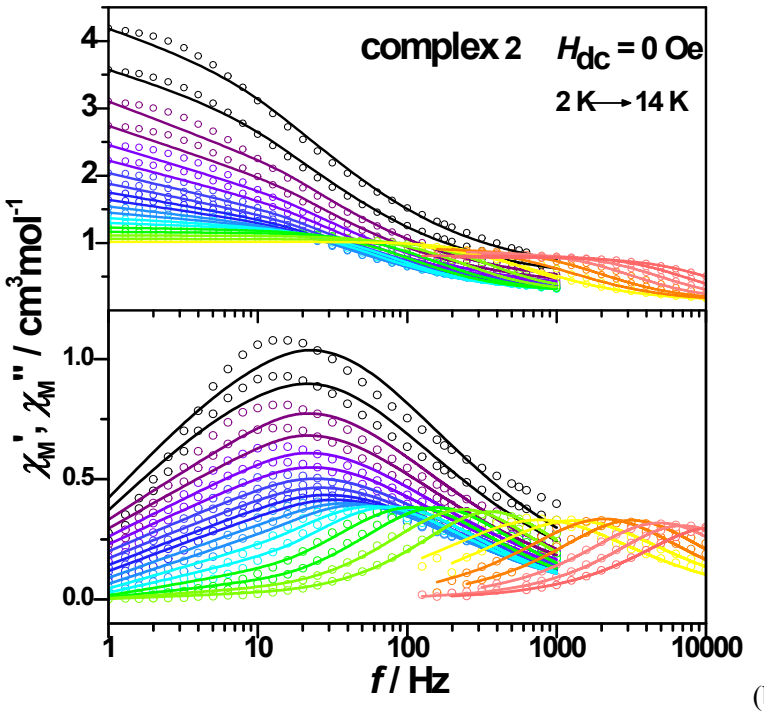
complex 2
H_{dc} = 0 Oe
2 K→14 K
χ_M', χ_M'' / cm^{3}mol^{-1}
f / Hz

(b)

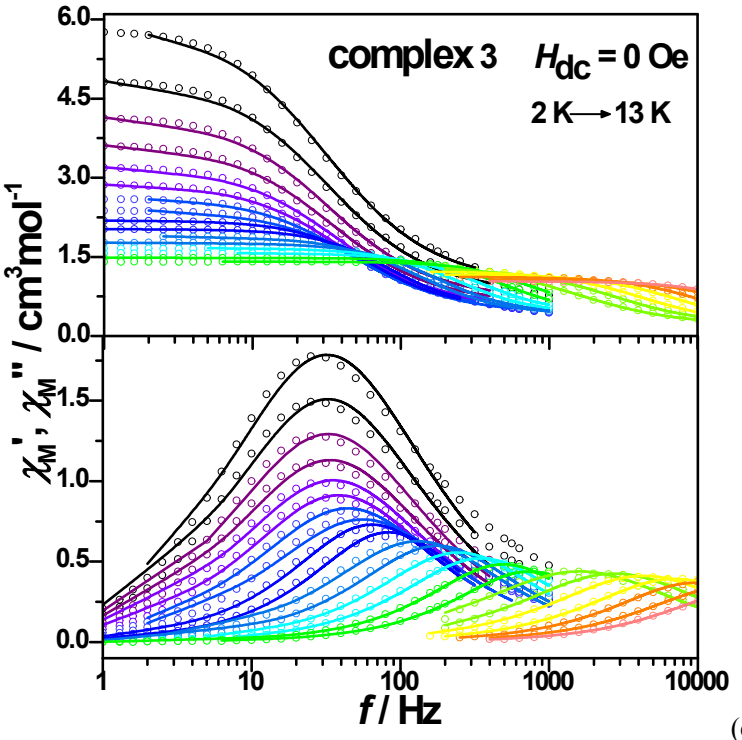

(c)

Fig. S9 Frequency dependence of the in-phase (top) and out-of-phase (bottom) ac susceptibility signal measured under zero dc field for **1**-**3**. Solid lines were fitted using a generalized Debye relaxation model, simultaneously to χ_M' (f) and χ_M'' (f) curves.

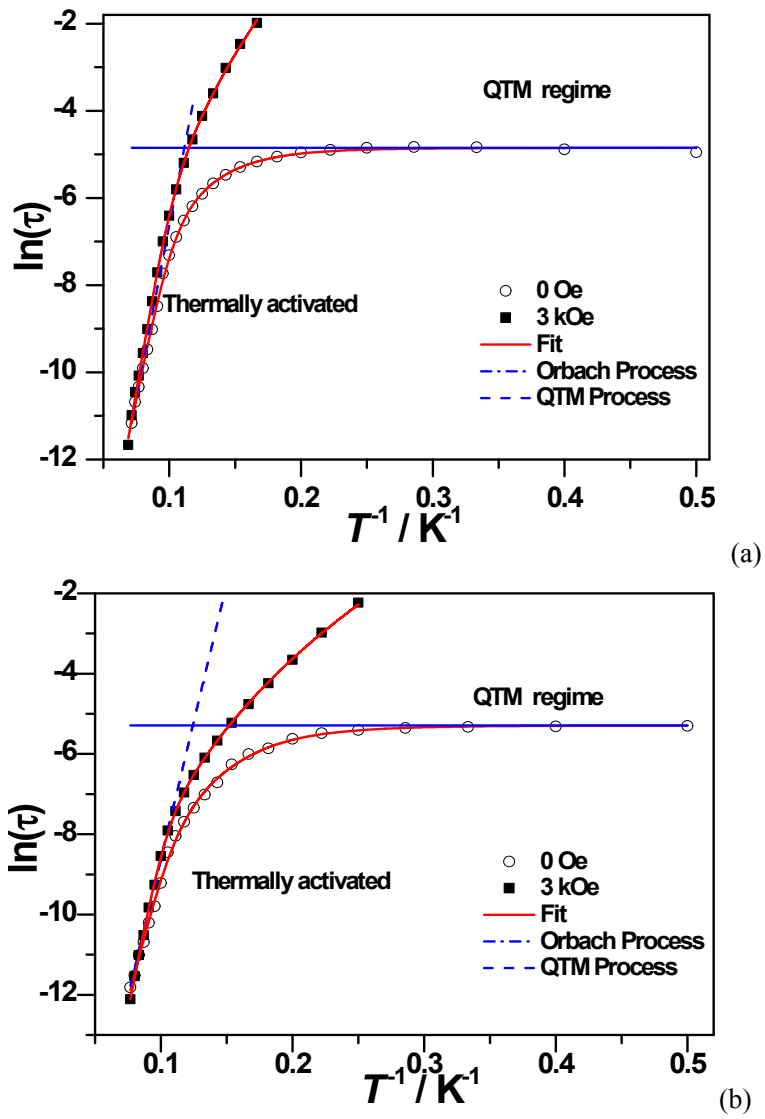

Fig. S10 Plot of ln(τ) *vs.* $T^{-1}$of complex **2** (a) and **3** (b). The red lines represent the fitting results. The dashed line represents the Orbach-type process

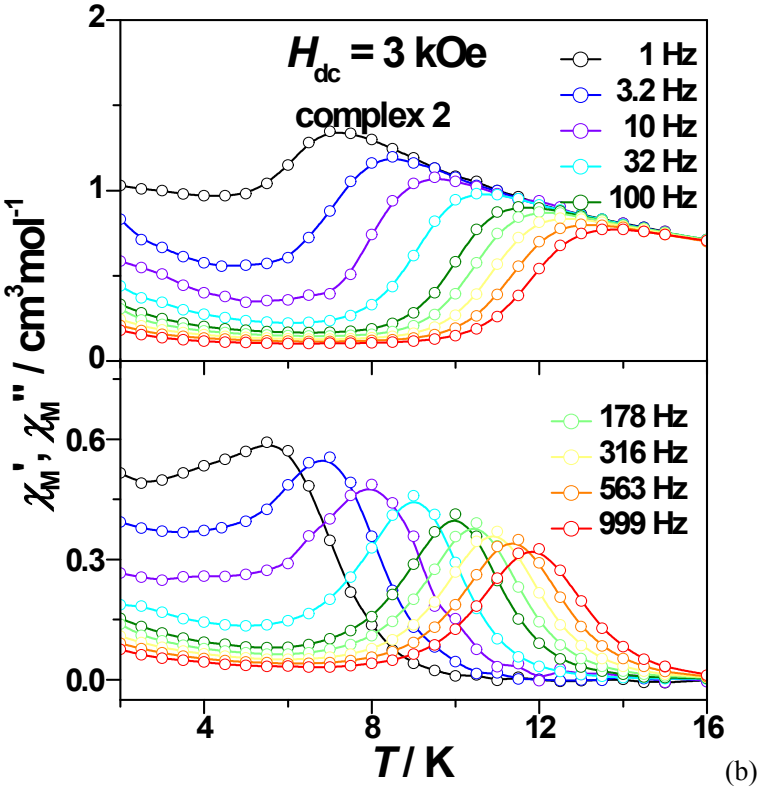

(b)

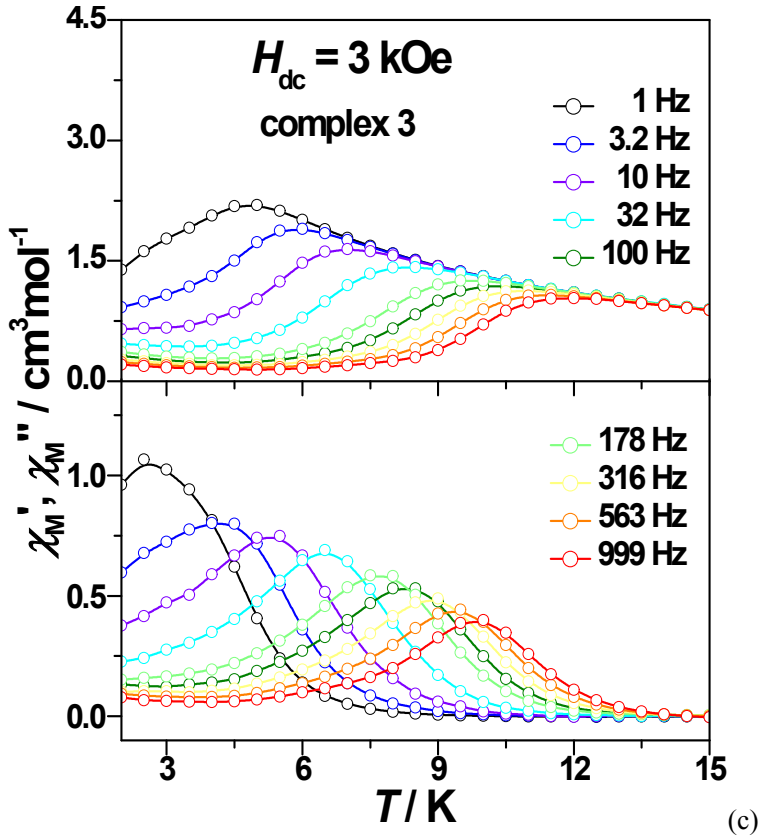

(c)

Fig. S11 The temperature dependence of ac susceptibility under 3 kOe for **2** and **3**.

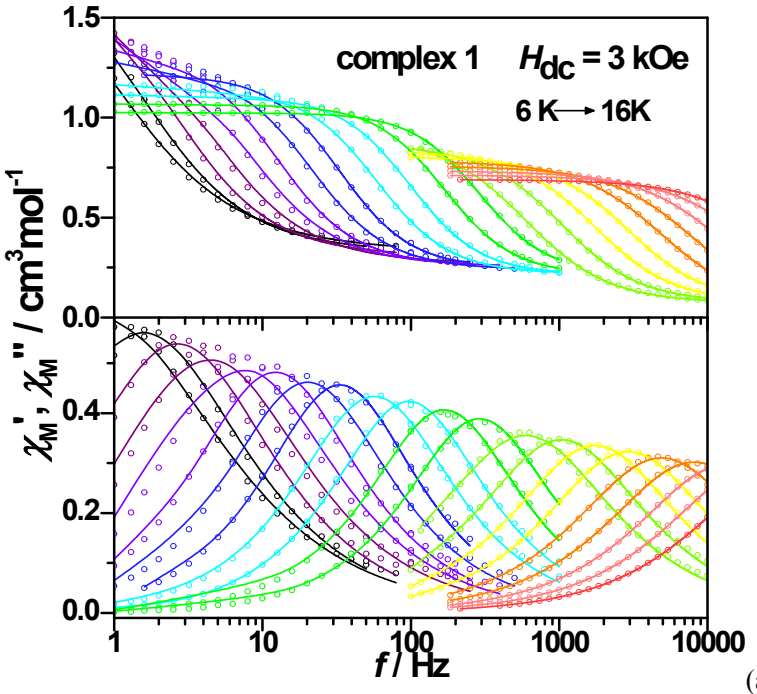
complex 1
H_{dc} = 3 kOe
6 K → 16K
χ_M', χ_M'' / cm^{3}mol^{-1}
f / Hz

(a)

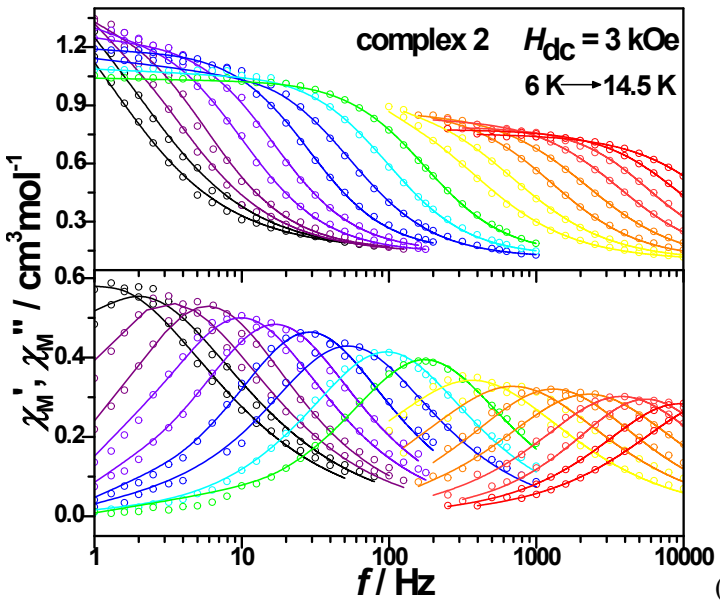
complex 2
H_{dc} = 3 kOe
6 K → 14.5 K
χ_M', χ_M'' / cm^{3}mol^{-1}
f / Hz

(b)

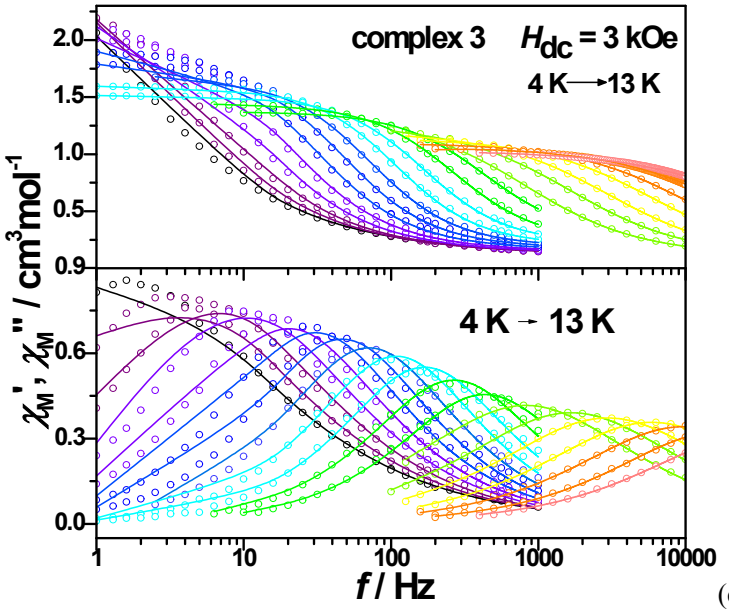

(c)

Fig. S12 Frequency dependence of the in-phase (top) and out-of-phase (bottom) ac susceptibility signal under 3 kOe dc field for **1**-**3**. Solid lines were fitted using a generalized Debye relaxation model, simultaneously to $\chi_M'(f)$ and $\chi_M''(f)$ curves.

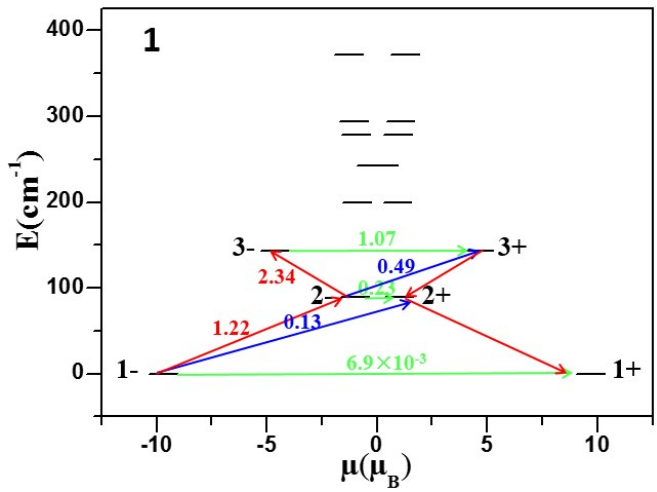

(a)

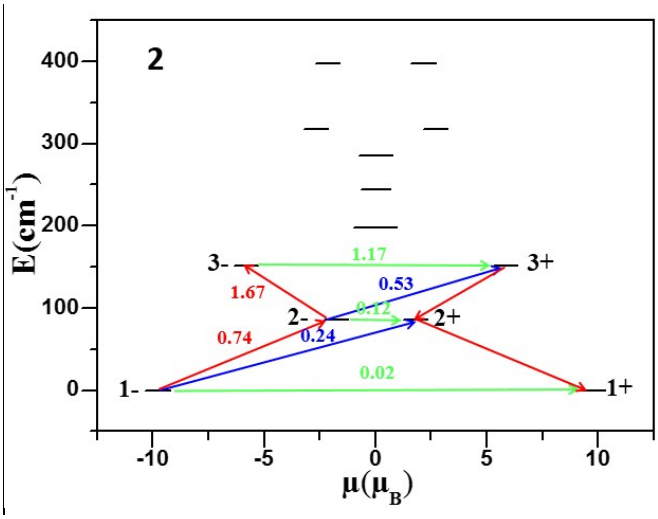

(b)

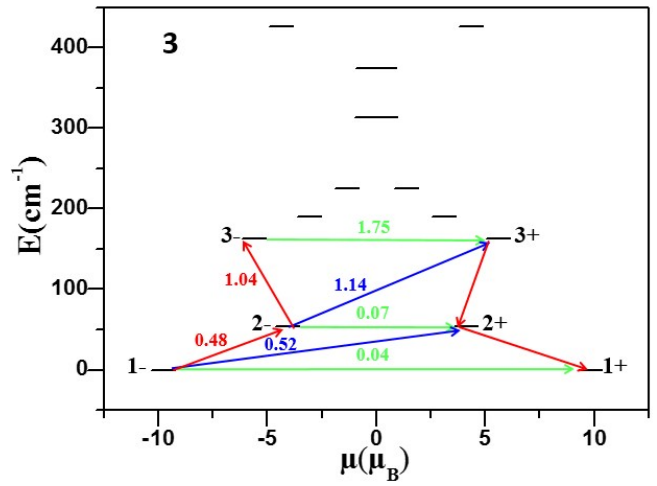

(c)

Fig. S13 The magnetization blocking barriers in complexes **1-3**. The thick black lines represent the Kramers doublets as a function of their magnetic moment along the magnetic axis. The green lines correspond to diagonal quantum tunneling of magnetization (QTM); the blue line represent off-diagonal relaxation process. The numbers at each arrow stand for the mean absolute value of the corresponding matrix

element of transition magnetic moment.

Reference

(1) Karlström, G.; Lindh, R.; Malmqvist, P. Å.; Roos, B. O.; Ryde, U.; Veryazov, V.; Widmark, P. O.; Cossi, M.; Schimmelpfennig, B.; Neogrady, P.; Seijo, L.; MOLCAS: A Program Package for Computational Chemistry. *Comput. Mater. Sci*. **2003**, 28, 222-239.

(2) Lines, M. E.; Orbital Angular Momentum in the Theory of Paramagnetic Clusters. *J. Chem. Phys*. **1971**, 55, 2977-2984.

(3) (a) Mondal, K. C.; Sundt, A.; Lan, Y. H.; Kostakis, G. E.; Waldmann, O.; Ungur, L.; Chibotaru, L. F.; Anson, C. E.; Powell, A. K.; Coexistence of Distinct Single-Ion and Exchange-Based Mechanisms for Blocking of Magnetization in a $Co^{II}_2Dy^{III}_2$ Single-Molecule Magnet. *Angew. Chem. Int. Ed*., **2012**, 51, 7550-75540. (b) Langley, S. K.; Wielechowski, D. P.; Vieru, V.; Chilton, N. F.; Moubaraki, B.; Abrahams, B. F.; Chibotaru, L. F.; Murray, K. S. A $\{Cr^{III}_2Dy^{III}_2\}$ Single-Molecule Magnet: Enhancing the Blocking Temperature through 3d Magnetic Exchange. *Angew. Chem. Int. Ed*., **2013**, 52, 12014-12019.

(4) (a) Chibotaru, L. F.; Ungur, L.; Soncini, A. The Origin of Nonmagnetic Kramers Doublets in the Ground State of Dysprosium Triangles: Evidence for a Toroidal Magnetic Moment. *Angew. Chem. Int. Ed.* **2008**, *47*, 4126-4129; (b) Ungur, L.; VandenHeuvel, W.; Chibotaru, L. F. Ab initio investigation of the non-collinear magnetic structure and the lowest magnetic excitations in dysprosium triangles. *New. J. Chem.* **2009**, *33*, 1224-1230; (c) Chibotaru, L. F.; Ungur, L.; Aronica, C.; Elmoll, H.; Pilet, G.; Luneau, D. Structure, Magnetism, and Theoretical Study of a Mixed-Valence $Co^{II}_3Co^{III}_4$ Heptanuclear Wheel: Lack of SMM Behavior despite Negative Magnetic Anisotropy. *J. Am. Chem. Soc.* **2008**, *130*, 12445-12455.